

## CARBON AND GRAPHITE MATRICES IN CARBON-CARBON COMPOSITES: AN OVERVIEW OF THEIR FORMATION, STRUCTURE, AND PROPERTIES

Gerald Rellick  
Mechanics and Materials Technology Center, Technology Operations  
The Aerospace Corporation, P.O. Box 92957, Los Angeles, CA 90009

**Keywords:** Carbon-carbon composites, Graphitization, Composite properties

### WHY CARBON-CARBON COMPOSITES?

Carbon-carbon (C/C) composites, so-called because they combine carbon-fiber reinforcement in an all-carbon matrix, can best be viewed as part of the broader category of carbon-fiber-based composites, all of which seek to utilize the light weight and exceptional strength and stiffness of carbon fibers. However, in C/C, the structural benefits of carbon-fiber reinforcement are combined with the refractoriness of an all-carbon materials system, making C/C composites the material of choice for severe-environment applications, such as atmospheric reentry, solid rocket motor exhausts, and disc brakes in high-performance military and commercial aircraft. Their dimensional stability, laser hardness, and low outgassing also make them ideal candidates for various space structural applications.

Such mechanical and refractory properties are not met by the various bulk graphites for two reasons: (1) graphites are very flaw sensitive and, therefore, brittle; and (2) graphites are difficult to fabricate into large sizes and complex shapes. These difficulties are largely overcome by taking advantage of the "two phase principle of material structure and strength [1]."

In the classical two-phase materials system, or composite, a high-strength, high-modulus, discontinuous-reinforcement phase is carried in a low-modulus, continuous-matrix phase; e.g., graphite fibers in a thermo-plastic-resin matrix. The stress in a composite structure having fiber reinforcement that is continuous in length, is carried in proportion to the moduli of the constituent phases, weighted by their respective volume fractions. Therefore, the much stiffer (higher-modulus) fibers will be the principal load bearers, and the matrix, in addition to having the task of binding together the composite, will deform under load and distribute the majority of stress to the fibers. At the same time, because the brittle carbon fibers are *isolated*, the possibility that an individual fiber failure will lead to propagation and catastrophic failure is practically eliminated.

Another major benefit of composites is that they permit the construction of complex geometries, and in such a way that different amounts of the load-carrying fibers can be oriented in specific directions to accommodate the design loads of the final structure. Closely associated with this "tailoring" feature of composites is that carbon-fiber technology enables exploitation of the exceptional basal-plane stiffness (and strength, in principle, although this is still much farther from realization) of  $sp^2$  bonded carbon atoms—i.e., the fibers are not isotropic, but rather have their graphite basal planes oriented preferentially in the fiber axial direction.

For very-high-temperature carbon-fiber-composite applications, say, above 2000°C, even for brief periods of time, it is necessary to employ a carbon matrix; however, like the fiber, the carbon matrix is also brittle. When fiber-matrix bonding is very strong in C/C, brittle fracture is frequently observed. The explanation is that strong bonding permits the development of high crack tip stresses at the fiber-matrix interface; cracks that initiate in either fiber or matrix can then propagate through the composite. However, if the matrix or the fiber-matrix interface is very weak, or microcracked, then the primary advancing crack can be deflected at such weakened interfaces or cracks. This is the Cook-Gordon theory [2] for strengthening of brittle solids, which states, more specifically, that if the ratio of the adhesive strength of the interface to the general cohesive strength of the solid is in the right range, large increases in the strength and toughness of otherwise brittle solids may result. Therefore, good fiber strength utilization in a brittle-matrix composite like C/C depends on control of the matrix and interfacial structures.

The objective of this paper is to provide a brief overview of carbon and graphite matrices in C/C, with an emphasis on recent research on some of the more fundamental materials issues involved [3-7]. Much of what is presented is taken from our own published work, which has focused on understanding how the structure of

the carbon or graphite matrix, and fiber-matrix interphase region, is influenced by starting materials and processing methods, and, in turn, how these structures affect composite properties. For comprehensive reviews of C/C, the reader is referred to Fitzer [8,9] for an overview of the basic materials issues, and to McAllister and Lachman [10] for a thorough treatment of fabrication and processing issues. Less comprehensive but more recent reviews that build principally on those just cited but that also deal with more specialized topics, such as oxidation protection of C/C, are contained in Refs. 11-13.

### FIBER ARCHITECTURE AND PREFORM DENSIFICATION

The composites designer, in addition to being able to choose from a wide variety of fiber types, also has a large number of fiber architectures available. For high-performance C/C applications, continuous (in length) fiber reinforcement is integrated to produce either a two-dimensional (2-D) or three-dimensional (3-D) fabric preform. According to Ko [14], a fabric preform is defined as "an integrated fibrous structure produced by fiber entanglement or yarn interlacing, interlooping, intertwining, or [nonwoven] multiaxial placement."

The preform may be dry, i.e., unimpregnated, as in 3-D orthogonal block structures, in which the x, y, and z yarns are "laid-in" straight to produce a structure having about 60% void volume (see Fig. 1a). The yarns may also be pultruded, i.e., impregnated with a resin binder and formed into rigid rods.

Alternatively, the fabrics may be impregnated with a thermosetting-resin binder and then the fabric plies laid up to produce the desired component (Fig. 1b). Such a structure is still termed 2-D because of the lack of through-thickness reinforcement.

To produce a C/C, the carbon-resin composite is baked, or fired, to pyrolyze the organic matrix. If the fabric is initially impregnated with a state-of-the-art phenol formaldehyde resin system, we can expect to obtain a C/C part with approximately 25% residual porosity after baking. However, experience has shown that such porosity is excessive, and that significant improvement in properties will follow if the porosity is reduced to values in the 5-15% range, depending on the particular type of structure. Therefore, not only in the dry preform, but also in the pyrolyzed "prepreg" fabric, additional volume increments of carbon matrix must be introduced into the C/C structure. The introduction can be achieved by one or a combination of three densification processes: CVI, use of coal-tar and petroleum pitches, and use of thermosetting resins. As each of these processes is discussed in turn, we will explore its characteristic structural features and densification behavior, and effects on properties. This discussion will also be used as an opportunity to introduce and discuss the various C/C characterization tools and techniques: X-ray diffraction, laser Raman microprobe spectroscopy, density measurements, and, particularly, polarized-light microscopy, and scanning and transmission electron microscopy (SEM and TEM).

### CVI

The first method for C/C densification, chemical vapor infiltration (CVI) [15,16], involves the passage of a hydrocarbon gas, typically methane, through the porous preform at temperatures in the 1000-1200°C range, with resulting deposition of carbon in the open porosity. Such low-temperature CVI leads to three principal carbon microstructures as defined by polarized-light microscopy [17-19]: rough laminar (RL), smooth laminar (SL), and isotropic. Isotropic deposits are generally very low density and of little value in C/C densification. Examples of RL and SL carbons in a PAN-based carbon-fiber composite are shown in the polarized-light micrographs of Figs. 2a and b.

A characteristic feature of both the RL and SL carbons is the set of extinction crosses observed under cross-polarized light. Such crosses are a consequence of the oriented nature of the deposits; the carbon layer planes align preferentially along the fiber surface. The anisotropic structure leads to a condition of birefringence in which two of the three principal crystallographic axes of graphite oriented at 90 deg to each other have different indices of refraction. Examination of Figs. 2a and b reveals two patterns of RL and SL deposits, illustrating that not only the amount but the type of carbon deposition can vary throughout the structure, depending on local temperature and gas concentration gradients [17].

In addition to orientation, another important feature of carbon matrices is their graphitizability, which is a measure of the ease in converting the pyrolyzed carbon matrix product into crystalline graphite through high-temperature heat treatments in the ~2000–3000°C range. The state of graphitization can be assessed by a number of techniques, the most common of which is X-ray diffraction (XRD). However, in C/C it is usually very difficult to resolve the resultant composite diffraction response into the respective fiber and matrix responses, because both phases are carbon. A technique to circumvent the sample volume problem is laser Raman microprobe spectroscopy (LRMS). Although the interpretation of the Raman spectra is more ambiguous than with XRD, LRMS permits focusing of a visible-light beam, as small as 1 μm in diameter, on a region of the specimen while recording the Raman spectrum, which is active in carbon [20]. Useful structural information on a local scale can be obtained in principle.

One major difficulty with applying LRMS to composites is that the size of constituent phases is of the order of microns, making it necessary to prepare the specimens for examination using standard optical polishing techniques. Such polishing tends to damage the near-surface structures and leaves behind a thin layer of polishing debris. Since the probe depth of the optical beam is only about 50 nm [20], the Raman spectrum unfortunately becomes a function of the preparation technique [21–23].

A technique we have employed extensively and with good success, and which is an outgrowth of early work performed at Los Alamos Laboratories [24,25], involves SEM examination of specimens that have been polished and then cathodically etched with xenon. When the carbon structure is graphitic, and when the graphite layer planes are oriented perpendicular to the plane of section, we see, typically, a pronounced lamellar texture, as revealed for the inner- and outermost CVI layers in the C/C of Fig. 3. The lamellar texture is the result of differential etching rates of the various microstructural units, the exact nature of which is still not clear. The most likely mechanism is preferential removal at lower-density, less-ordered intercrystalline-type boundaries that separate regions of good crystalline registry; this is seen very dramatically in highly oriented pyrolytic graphites reacted in oxygen [26,27]. The technique is effective, principally, in distinguishing broadly between graphitic and nongraphitic carbon on a scale of microns.

Returning to Fig. 3, this particular specimen has the CVI deposition sequence RL/SL/RL (as determined separately from polarized-light microscopy) and has been heat-treated to 2500°C for 1 hr. The lamellar texture of the RL zones indicates their graphitized structure, whereas the absence of significant texture in the SL zone indicates that the SL structure is essentially glassy carbon. This observation was confirmed by XRD, LRMS, and by selected physical-property measurements [28]. The effect of having a graphitic and well-oriented matrix is illustrated by the higher thermal conductivities for heat-treated RL composites shown in Fig. 4.

Modulus enhancement is another interesting effect of a well-oriented, graphitic matrix (Fig. 5). For the particular pseudo-3-D, felt-based C/C composite of the figure, there were two CVI densifications. Following the first, the composite structure was heat-treated to 2500°C; the second CVI was left in the as-deposited state (~1000–1200°C). The relative proportions of the first and second CVI varied with each specimen, but the total CVI weights were approximately the same. The fiber volume (and weight) fraction was constant (~20%) for each composite.

The strong dependence of the modulus on the relative proportion of heat-treated CVI indicates that the carbon matrix can carry a significant fraction of the load, particularly, in this case, if the structure is heat-treated to typical graphitization temperatures. The modulus-enhancement effect by the matrix is especially striking in this composite because of the use of low-modulus fibers at fairly low volume fractions. However, as will be seen, this effect is an important materials and processing consideration in all C/C composites.

#### Coal-Tar and Petroleum Pitches

The second method for C/C densification is the use of coal-tar and petroleum pitches. Because they are thermoplastic, pitches are used mostly for redensification; i.e., further densifying of a C/C structure that has been "rigidized" by an earlier impregnation/densification step (e.g., a resin-impregnated fabric preform) or that has sufficient rigidity from the friction between the elements of the woven structure (e.g., 3-D braided preform).

Pitches are unique in passing through a liquid-crystalline transformation at temperatures between about 350 and 550°C [29]. In this transformation, large lamellar molecules formed by the reactions of thermal cracking and aromatic polymerization are aligned parallel to form an optically anisotropic liquid crystal known as the carbonaceous mesophase [30]. The alignment of the lamellar molecules is the basis for easy thermal graphitizability of the carbonized product. One of the features of a mesophase-based matrix is high bulk density, which is achievable because the matrix density can approach the value for single-crystal graphite, 2.26 g/cm<sup>3</sup>.

The topic of pitch impregnation and densification of C/C introduces the subject of densification efficiency, the most meaningful measure of which is *volumetric* densification efficiency [31]. It is the ratio of the volume of carbon matrix in a process cycle to the volume of porosity available for densification.

For pitches carbonized at atmospheric pressure, coke yields are of the order of 50–60%, impregnant densities are ~1.35 g/cm<sup>3</sup>, and, as we have noted, densities for pitch-derived matrices are ~2.2 g/cm<sup>3</sup>. From these values we calculate volumetric densification efficiencies of only 30–40% at atmospheric pressure [31]. By resorting to so-called hot isostatic-pressure-impregnation-carbonization (HIPIC), to pressures of about 15,000 psi, carbon yields of pitches can be increased to almost 90% [10]. But even with HIPIC, volumetric filling is only 55%. Therefore, given a preform with initial porosity of 45%, typical for many 3-D woven structures, three cycles at *maximum densification efficiency* would be required to reduce the porosity to 4%. With current HIPIC procedures, however, it is found that at least five cycles at 15,000 psi are required to achieve this same level of porosity. Such reduced efficiency in real systems is the result of forced expulsion of pitch from the preform as a result of the gas-forming pyrolysis reactions accompanying carbonization.

Clearly, one way to increase efficiency, for a given weight-based carbon yield, is to select either an impregnant or an HTT that will lower the final matrix density. As will be seen in the next subsection, lower-density carbon matrices can be achieved by using resin precursors that form a glassy-carbon-type structure. But, although this approach fills more of the available space, it does so with a lower-density carbon matrix, which is different in structure from the higher-density graphitic matrix. The trade-offs in properties, particularly mechanical, are not well understood. We will touch on this topic again in the next subsection.

Approaches to improving densification efficiency of pitch-based matrices without resorting to HIPIC processing include the use of heat-treated and solvent-extracted pitches [32] and partially transformed (to mesophase) pitches [33,34]. A novel approach, developed by White and Sheaffer [35], is to oxidatively stabilize the mesophase following impregnation and transformation, an approach similar to that employed in mesophase-fiber stabilization. The result is a "hardened" mesophase that is resistant to the bloating effects of pyrolysis gases but that, upon further heat treatment, yields a dense, graphitic carbon.

The strong orienting effect of the fiber surface on the large lamellar mesophase molecules is an interesting feature of mesophase formation in C/C composites. This effect was demonstrated by the work of Zimmer and Weitz [36], who used polarized-light microscopy to show that mesophase molecules near a fiber surface in a close-packed fiber bundle always aligned parallel to the fiber surfaces, even in the presence of strong magnetic fields. Singer and Lewis demonstrated earlier that magnetic fields would orient mesophase molecules in *bulk* mesophase [37]. Zimmer and Weitz showed that mesophase would also orient in matrix-rich regions within the fiber bundles—i.e., at points far removed from fiber surfaces [36]. They calculated a magnetic coherence length of 7 μm, which corresponds roughly to the distance over which the orientation effect acts.

Such localized orientation in the liquid-crystalline state would lead one to expect the final, graphitized matrix also to be well oriented in the immediate vicinity of the fiber. First observed by Evangelides [38] using SEM in conjunction with xenon-ion-etching, such a matrix "sheath effect" is depicted in Fig. 6 in a coal-tar-pitch-densified C/C.

Modulus enhancement in pitch-based C/C has been widely reported, but whether the effect is due to the matrix or to an increase in the fiber modulus, resulting from high-temperature heat-treatment-induced structural changes in the fiber, has not been clarified [39]. The sheath effect is also pronounced in resin-based carbon matrices, but for different reasons, which we will examine in the next subsection.

Matrix microcracking is characteristic of all C/Cs, but it is particularly prevalent in graphitic matrices because of the combination of weak shear planes in polycrystalline graphite and the thermal stresses generated during heat treatment (Fig. 7) [40,41]. Microcracking also has important effects on the engineering properties of C/C materials—particularly the matrix-dominated properties in the unreinforced directions, such as the interlaminar shear strength and perpendicular-to-ply tensile strength in 2-D C/C laminates. However, as mentioned above, such microcracking appears to improve in-plane flexural and tensile strength, by way of a Cook-Gordon mechanism [42-45].

### Thermosetting Resins

The third, and last, class of C/C impregnant to be discussed is thermoset resins, which are the basis for "prepreg" fabric and tapes, as noted above; resin systems can also be used for reimpregnation. In addition to their easy fabricability, thermosets have the advantage of "charring-in-place;" that is, although they soften and deform on heating, they do not fuse or liquefy, and, therefore, no special tools or techniques must be employed to retain the matrix in the composite during pyrolysis.

Thermoset resins are usually highly crosslinked, which makes them resistant to thermal graphitization *in bulk form*, even to temperatures of 3000°C [5,46]. Phenolic resins are currently most commonly used for prepreg operations, whereas furan-based resins are used more for reimpregnating. Both have char yields typically in the 50-60% range.

The development of ultra-high-char-yield resins derived from polymerization of diethynylbenzene (DEB) [47-51], usually termed polyarylacetylenes (PAA) [47], has received much focus in recent years. The structure of DEB is illustrated in Fig. 8, along with a synthesis route that involves a catalytic cyclotrimerization prepolymerization in methyl ethyl ketone solvent [48,49]. The cyclotrimerization liberates much of the exothermic heat of polymerization, thereby allowing safe, controllable curing. The principal appeal of PAAs is their extremely high char yield. From the average structure, we calculate a theoretical carbon yield of about 95%; in practice, PAAs can have carbon yields of 90% to 700°C, although more practical formulations employing monofunctional chain terminators to improve flow properties reduce this yield to about 85% [48,49].

Similar to other crosslinked thermosets, PAAs produce largely nongraphitizable carbons. To extend the range of matrix structures for this fabricable resin system, we have been exploring approaches to *in situ* matrix catalytic graphitization in C/C in our laboratory. One promising approach, by Zaldivar *et al.* [52], has been the use of boron in the form of a carborane compound. Figure 9a is a plot of room-temperature tensile strength of undoped and boron-doped unidirectional C/Cs versus HTT; the strengths are calculated relative to the fiber cross-sectional areas on the assumption that the matrix carries negligible load relative to the fibers. The strength of the fibers in the cured-resin composite is taken to be the value for full strength utilization. The plot illustrates a number of important features. First, for the undoped system, strength exhibits a large decrease as the composite proceeds from cure to carbonization, owing to conversion of the compliant polymer matrix into a well-bonded, low-strain-to-failure carbon matrix. Increasing boron levels lead to increased strength utilization for the 1100°C HTT samples: The undoped specimen behaves as a monolithic solid and fractures in a planar-catastrophic mode (Fig. 10a); the 5% B-doped samples exhibit extensive fiber pullout (Fig. 10b), which indicates a weakened interface. The reasons for the weakened interface are unclear, since X-ray diffraction revealed no significant difference in graphitization between doped and undoped specimens after this HTT.

At higher HTTs, the use of higher boron levels leads to a reduction in strength utilization (and an increase in modulus; Fig. 9b), due to catalytic graphitization of the fiber. Further HT of the undoped specimens beyond 1100°C "reclaims" much of the lost fiber strength, for the reasons discussed above. More work is needed to define the mechanisms by which catalytic graphitization of the matrix affects the properties of C/C.

We recently reported a striking modulus enhancement for the same type of 1-D composite studies (Zaldivar *et al.* [7]), using four mesophase-based fibers from DuPont and PAA resin (Fig. 11). The number in the fiber designation is the axial tensile modulus, in Mpsi. For HT to 2750°C, all the composites exhibit sharp increases in fiber moduli, to values exceeding 150 Mpsi, which is the theoretical limit of the graphite basal-plane modulus. Since the moduli are calculated relative to the original fiber cross-sectional areas, such values

indicate that the composite modulus must have significant contributions from the matrix. An example of a matrix sheath that may be contributing to the composite modulus is shown in Fig. 12.

This figure brings us to the subject of stress-induced orientation and graphitization in otherwise nongraphitizing carbon matrices in C/C. While the phenomenon of stress graphitization of hard carbons has been noted for some time [24,25,53,54], only recently have serious efforts have been made to understand the physical-mechanical mechanisms involved in matrix orientation and graphitization in C/C [5,6,55]. This topic is of more than academic interest, because the formation of a two-phase matrix of graphitic and nongraphitic, oriented and unoriented, zones can have a major influence on the mechanical properties of C/C composites.

To examine preferred orientation in thermosetting-resin-impregnated matrices, cross sections of C/C tows fabricated from Amoco T50 PAN-based fibers and a PAA resin were polished, then heat-treated to 2900°C for 1 hr and xenon-ion-etched. The polarized-light micrograph of Fig. 13a reveals that in addition to the pronounced lamellar zones, the smooth-appearing zones—which, by definition, have formed no observable texture with etching—are nevertheless oriented, as evidenced by the polarized-light extinction contours sweeping across the surface of the sample as the analyzer is rotated. We conclude that even the thickest ( $> 20 \mu\text{m}$  matrix regions in this specimen are oriented. Pronounced optical anisotropy in the matrix for the same composite heat-treated to only 1200°C is revealed by Fig. 13b. As expected, etching produced no lamellar texture for this low HTT.

The highly localized nature of the combination of stress-induced orientation and graphitization is one of its more interesting features: i.e., all of the carbon matrix in the specimen of Fig. 13a is oriented to some degree, yet only certain discrete regions become lamellar graphite upon HT to 2900°C. SEMs of ion-etched specimens reveal this localized graphitization more clearly (Fig. 14); particularly striking is the shrinkage of the matrix away from the fiber, which is a result of the volume decrease accompanying graphitization.

TEM is an extremely effective technique for studying the local structure on an even finer scale. In the transverse (Fig. 15a) and longitudinal (Fig. 15b) bright-field images of thin sections of a T50 fiber/resin-derived C/C heated to 2750°C, crystallite formation and orientation are evident, particularly in the transverse section (compare with Fig. 13a). Selected area electron diffraction confirmed the highly crystalline structure of the interfilament matrix regions [56].

In the SEM of Fig. 16a, we observe an interesting effect: At the interstice of five contiguous fibers there is no lamellar formation in the matrix pocket, except perhaps immediately adjacent to the filament surfaces. This effect was typically observed in close-packed groups of three to five fibers. In contrast, in more extensive matrix regions—for example, those that bound two relatively fiber-rich areas, and where the matrix boundaries are fairly straight—we observe relatively unimpeded development of lamellar structure over a distance of several microns (Fig. 16b). Such lamellar development is particularly striking at the extreme outside of the single-tow specimens where quite thick ( $\sim 1\text{--}2$  fiber diameters) lamellar zones form (Fig. 16c). In Fig. 16d, we see that an interruption in the uniformity of the interface between this outer matrix crust and the composite leads to a transition from the lamellar to nonlamellar structure.

Further microstructural features not seen in polished specimens are revealed in the SEM of a tensile-fracture surface (Fig. 17). The lamellar regions in the matrix are still evident, and the PAN-based fibers show their typical fibrillar structure. But we now observe in the matrix both lamellar and fibrillar textures, the latter resembling that seen in the T50 fibers, which are generally considered to be oriented glassy carbon [46].

Two observations suggested to us that the key factor in determining lamellar-structure formation in a C/C composite matrix is a *multiaxial* deformation of the resin during its pyrolysis to carbon. First, consider that, in normal PAN-fiber manufacture, which leads to a fibrillar structure, the filaments are subjected to a uniaxial tensile stress during oxidation stabilization. However, when carbonized without prior oxidation stabilization, but in *very thin sections*, such as between the layers of montmorillonite clay, PAN has been shown to yield a single-crystal structure following subsequent graphitization heat treatment [57]. Second, in partially oxidized (through-the-thickness) PAN fibers, the unoxidized, fusible core can form lamellar carbon [58].

In both examples, the mechanical restraints imposed on the PAN during its pyrolysis would be expected to produce multiaxial deformation. In this critical regime, a number of stresses act at the fiber-matrix interface, assuming good fiber-matrix adhesion: First, there is an axial tensile stress that acts on the matrix; it is a consequence of the large matrix pyrolysis shrinkage, and the high axial modulus and low axial thermal expansion of the fiber. This matrix shrinkage also generates two additional matrix stresses in the plane perpendicular to the axial direction—a compressive stress, which acts radially, and a tensile stress, which acts circumferentially.

We tested this hypothesis by performing a linear elastic plane-strain thermal stress analysis for three different local fiber-matrix composite configurations: a clustered arrangement of three fibers and four fibers, sketched in Figs. 18a and b, respectively, and a matrix with free boundaries. These three cases correspond closely to those seen in Figs. 16a-d. The material properties used for the PAN fiber and phenolic-resin matrix are typical values obtained from a variety of sources. The mechanical properties of the pyrolyzing matrix are those reported by Fitzer and Burger [59]. The thermal environment was a heatup from room temperature to 1000°C.

In the analysis we are concerned only with the stresses in the matrix in the plane perpendicular to the fiber axis, because the tensile stress of the matrix in the fiber direction at any point in the matrix is clearly more or less constant at a given temperature owing to the plane-strain consideration. The stresses in the radial-tangential plane may vary significantly, depending on their relative location to the fiber. At any point in the matrix, therefore, we have a state of triaxial stress.

The development of lamellar structure in the matrix was postulated to be favored by two factors: (1) a large value of the maximum tensile stress in the plane, and (2) a small value of the ratio of minimum-to-maximum principal stress in this same plane. That is, for a given value of maximum tensile stress in the matrix, lamellar formation is favored more when the minimum-to-maximum stress ratio at any location is either small or negative (i.e., compressive). These two parameters may vary with the fiber spacing and boundary conditions, e.g., constrained or free edge.

Figure 19a, a plot of principal stress orientation and relative stress magnitudes, indicates that the maximum stress adjacent to the outside diameter of each fiber is dominated by hoop tension with a very low level of radial tensile stress; by contrast, the maximum stress in the center of the pocket is equal to about one-third that at the fiber surface, and the minimum (tensile) stress is now significant. From our hypothesis, these two factors will work in the direction of reduced lamellar formation relative to that at the fiber surface.

The effects of an increase in the  $a/r$  ratio (Fig. 18) are to decrease the maximum hoop stress at the fiber-matrix boundary and increase the stress ratio in the pocket region. In other words, when the three fibers are more closely packed, the formation of lamellar structure at the fiber surface is more favored than when they are loosely packed; however, within the pocket, it is less favored. Similar results were found for the four-fiber case.

We used the model of Fig. 18b to make the calculation for the free-boundary condition occurring along a straight, resin-rich area; the stress in the matrix along the free boundary is primarily unidirectional. Figure 19b illustrates that the relative stress magnitude and orientation correlate with the location of formation of lamellar structure depicted in Fig. 16c.

In conclusion, it is seen that the magnitude and orientation of the matrix shrinkage stresses during pyrolysis, as estimated by this analysis, are consistent with the proposed model for stress orientation and graphitization.

Much still remains to be learned about matrix stress graphitization in C/C: e.g., the effects of fiber type, fiber volume, matrix precursor, and high-temperature creep deformation. Equally intriguing is the possibility of being able to control C/C properties by controlling the matrix orientation and graphitization behavior.

## SUMMARY

Carbon-carbon composites are an exceptional class of high-strength, low-weight refractory materials; however, effective utilization of the carbon fiber properties requires appropriate selection of the carbon or graphite matrix and processing conditions. The matrices may be derived from hydrocarbon gases, coal-tar and petroleum pitches, and thermosetting resins, and represent a range of structures and properties. Current research is beginning to elucidate how C/C composite properties may be controlled by controlling the structures of the matrix, both in bulk matrix regions and, more sensitively, at the crucial fiber-matrix interphase region.

## ACKNOWLEDGMENTS

This paper reviews selected aspects of work funded by the Air Force Space Systems Division under Contract No. F04701-88-C-0089, and by the Aerospace Sponsored Research Program. The author wishes to thank a number of coworkers: Rafael Zaldivar, particularly, who, as an Aerospace MS and PhD Fellow, is responsible for much of the work discussed here; Dr. Dick Chang for his effective collaboration on portions of this work; and Paul Adams, Jim Noblet, Ross Kobayashi, Joe Uht, Dick Brose, and Ca Su, all of whom contributed in significant ways.

## REFERENCES

1. Slayter, G., *Sci. Am.*, 124 (January 1962).
2. Cook, J., and Gordon, J. E., *Proc. R. Soc. London A282*, 508 (1964).
3. Jortner, J., *Effects of Weak Interfaces on Thermostructural Behavior of C-C Composites*, Office of Naval Research, Annual Report, pp. 19-31 (March 1985).
4. Peebles, L. H., Meyer, R. A., and Jortner, J., In *Interfaces in Polymer, Ceramic and Metal Matrix Composites*, H. Ishida, Ed., p. 1, Elsevier (1988).
5. Zaldivar, R. J., and Rellick, G. S., "Some Observations on Stress Graphitization in C-C Composites," *Carbon* (in press).
6. Rellick, G. S., Chang, D. J., and Zaldivar, R. J., *Ext. Abstr., 20th Carbon Conf.* (1991), p. 404.
7. Zaldivar, R. J., Rellick, G. S., and Yang, J., *Ext. Abstr., 20th Carbon Conf.* (1991), p. 400.
8. Fitzer, E., *Carbon* 25, 163 (1987).
9. Fitzer, E., and Huttner, W., *J. Phys. D: Appl. Phys.* 14, 347 (1981).
10. McAllister, L. E., and Lachman, W. In *Handbook of Composites*, A. Kelly and S. T. Mileiko, Eds., Vol. 4, p. 109, Elsevier (1983).
11. Hsu, S. E., and Chen, C. I., In *Superalloys, Supercomposites and Superceramics*, p. 721, Academic Press (1989).
12. Buckley, J. D., *Ceram. Bull.* 67, 364 (1988).
13. Strife, J. R., and Sheehan, J. E., *Ceram. Bull.* 67, 369 (1988).
14. Ko, F., *Ceram. Bull.* 68, 401 (1989).
15. Bokros, J. C., In *Chemistry and Physics of Carbon*, P. L. Walker, Jr., Ed., Vol. 5, p. 1, Dekker, NY (1969).
16. Kotlensky, W. V., In *Chemistry and Physics of Carbon*, P. L. Walker, Jr., Ed., Vol. 9, p. 173, Dekker, NY (1973).
17. Pierson, H. O., and Lieberman, M. L., *Carbon* 13, 159 (1975).
18. Granoff, B., *Carbon* 12, 405 (1974).
19. Loll, P., Delhaes, P., Pacault, A., and Pierre, A., *Carbon* 15, 383 (1977).
20. (a) Tuinstra, F., and Koenig, J., *J. Chem. Phys.* 53, 1126 (1970); (b) *J. Compos. Mater.* 4, 492 (1970).
21. Miller, T. G., Fischbach, D. B., and Macklin, J. M., *Ext. Abstr., 12th Carbon Conf.* (1975), p. 105.
22. Vidano, R., and Fischbach, D. B., *Ext. Abstr., 15th Carbon Conf.* (1981), p. 408.
23. Katagiri, G., Ishida, H., and Ishitani, A., *Carbon* 26, 565 (1988).
24. Chard, W. C., Reiswig, R. D., Levinson, L. S., and Baker, T. D., *Carbon* 6, 950 (1968).
25. Reiswig, R. D., Levinson, L. S., and O'Rourke, J. A., *Carbon* 6, 124 (1968).
26. Rodriguez-Reinoso, F., and Thrower, P. A., *Carbon* 12, 269 (1974).
27. Rellick, G. S., Thrower, P. A., and Walker, P. L., Jr., *Carbon* 13, 71 (1975).
28. Rellick, G. S., *Ext. Abstr., 20th Carbon Conf.* (1991), p. 368.

29. Brooks, J. D., and Taylor, J. H., *Nature* **206**, 697 (1965).
30. White, J. L., In *Prog. Solid State Chem.*, J. O. McCauldin and G. Somarjai, Eds., Vol. 9, p. 59, Pergamon Press (1975).
31. Rellick, G. S., *Carbon* **28**, 589 (1990).
32. Zimmer, J. E., and Salvador, L. M., U.S. Patent 4,554,024 (19 November 1985).
33. Brückmann, H., Dr.-Ing Thesis, University of Karlsruhe (1979).
34. Singer, L. S., Lewis, I. C., and Bacon, R., *Proceedings of the JANNAF Rocket Nozzle Technology Subcommittee Meeting*, Naval Surface Warfare Center, Silver Spring, MD (17-19 October 1989).
35. White, J. L., and Sheaffer, P. M., *Carbon* **27**, 697 (1989).
36. Zimmer, J. E., and Weitz, R. L., *Carbon* **26**, 579 (1988).
37. Singer, L. S., and Lewis, R. T., *Ext. Abstr., 11th Carbon Conf.* (1973), p. 207.
38. Evangelides, J. S., *Ext. Abstr., 12th Carbon Conf.* (1975), p. 93.
39. Jortner, J., Appendix A in Ref. 3 above.
40. Jortner, J., In *Proc. Army Symp. on Solid Mechanics*, AMMRC MS 76-2 (1976), pp. 81-97.
41. Jortner, J., *Carbon* **24**, 603 (1986).
42. Buch, J. D., *Structure-Property Relationships in Advanced Carbon Materials*, Report No. TOR-0079(4726-04)-1, The Aerospace Corporation, El Segundo, CA (25 September 1979).
43. Manocha, L. M., and Bahl, O. P., *Carbon* **26**, 13 (1988).
44. Manocha, L. M., Yasuda, E., Tanabe, Y., and Kimura, S., *Carbon* **26**, 333 (1988).
45. Meyer, R. A., and Gyetvay, S. R., In *Petroleum Derived Carbons*, J. Bacha, J. Newman, and J. L. White, Eds., ACS Symp. Series **303**, p. 380, ACS (1986).
46. Jenkins, G., Kawamura, K., and Ban, L. L., *Proc. R. Soc. London* **A327**, 501 (1972).
47. Jabloner, H., U.S. Patent No. 4,070,333 (24 January 1978).
48. Barry, W. T., Gaulin, C., and Kobayashi, R., *Review of Polyarylacetylene Matrices for Thin-Walled Composites*, Report No. TR-0089(4935-06)-1, The Aerospace Corporation, El Segundo, CA (25 September 1989).
49. Katzman, H. A., *Polyarylacetylene Resin Composites*. TR-0090(5935-06)-1, The Aerospace Corporation, El Segundo, CA (2 April 1990).
50. Zaldivar, R. J., Rellick, G. S., and Yang, J. M., "Processing Effects on the Mechanical Behavior of Polyarylacetylene-Derived C-C." *SAMPE J.* (in press).
51. Brown, S. C., and Reese, H. F., *Proc. JANNAF RNTS Mtg.*, CPIA Publ. No. 496, Patrick AFB, FL (1986).
52. Zaldivar, R. J., Kobayashi, R., Rellick, G. S., and Yang, J. M., "Carborane-Catalyzed Graphitization in Polyarylacetylene-Derived C-C." *Carbon* (in press), and *Ext. Abstr., 20th Carbon Conf. (1991)*, p. 388.
53. Franklin, R. E., *Proc. R. Soc. London* **A209**, 196 (1951).
54. Hishiyama, Y., Inagaki, M., Kimura, S., and Yamada, S., *Carbon* **12**, 249 (1974).
55. Kimura, S., Tanabe, Y., Takase, N., and Yasuda, E., *Jpn. J. Chem. Soc.* **9**, 1479 (1981).
56. Rellick, G. S., and Adams, P. M., Aerospace Sponsored Research Program unpublished results.
57. Kyotani, T., Sonobe, N., and Tomita, A., *Nature* **331**, 331 (1988).
58. Johnson, J. W., Rose, P. G., and Scott, G., *Third Conf. on Indust. Carbons and Graphites*, SCI, London (1971), p. 443.
59. Fitzer, E., and Burger, A., In *Carbon Fibers: Their Composites and Applications* **134**, The Plastics Inst., London (1971).

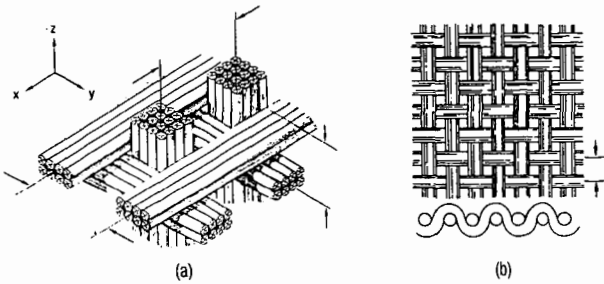


**Figure 1.** Schematic of (a) 3-D block construction and (b) 2-D plain-weave fabric (McAllister and Lachman [10]).

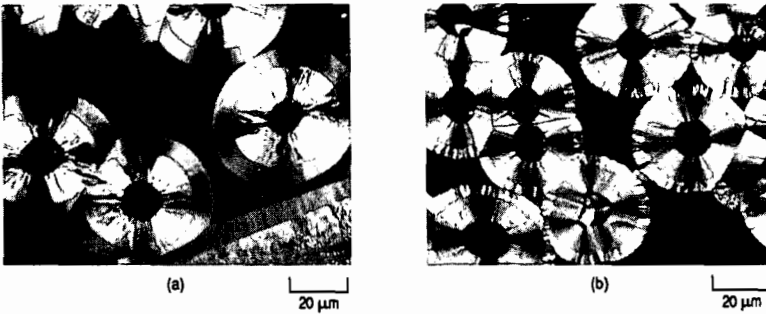


**Figure 2.** Polarized-light micrographs showing as-deposited CVI carbon microstructures of two specimens. Deposition sequence: (a) RL/SL; (b) SL/RL (Rellick [28]).

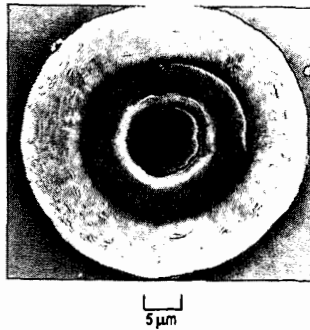


**Figure 3.** Scanning electron micrograph of specimen after heat treatment at 2500°C for 1 hr [28].

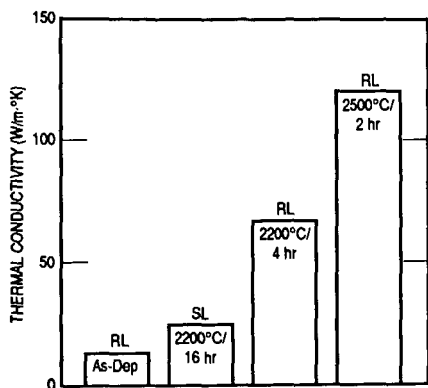


Figure 4. Through-thickness thermal conductivity (at RT) for composite specimens of different CVI structures and processing stages [28].

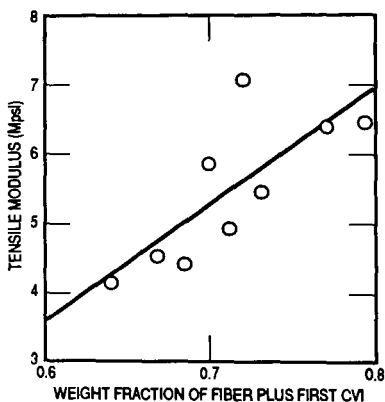


Figure 5. Composite tensile modulus versus weight fraction of fiber plus heat-treated CVI [28].

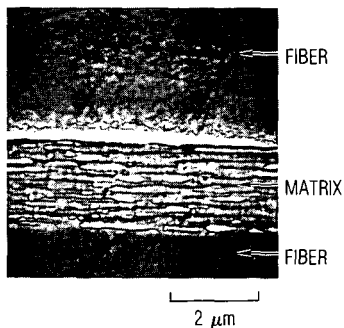
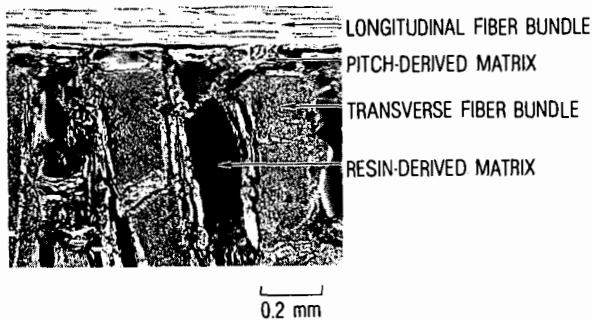
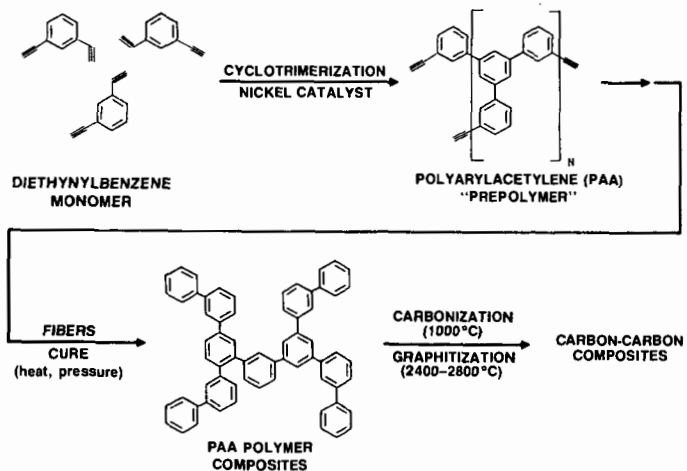


Figure 6. SEM showing highly aligned coal-tar-pitch-derived graphite matrix in the interfilament region of a C/C composite. Fibers are Amoco T50 from PAN.



**Figure 7.** Optical micrograph of cross section of 3-D C/C composite densified with both pitch and resin and heat-treated to 2750°C. Note extensive matrix microcracking.



**Figure 8.** Chemical structure and processing of PAA-based composites (Barry *et al.* [48] and Katzman [49]).

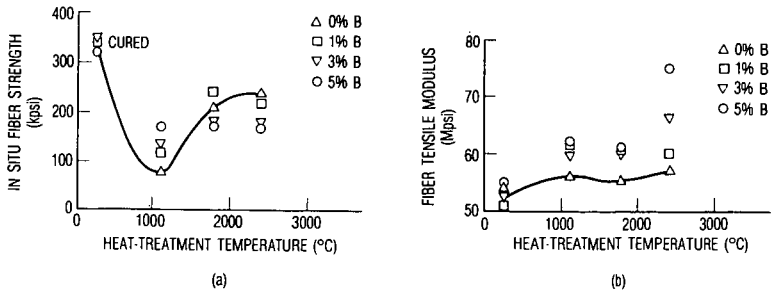


Figure 9. Plots of tensile (a) strength and (b) fiber modulus of undoped and B-doped PAA/T50 C/C composites (Zaldivar *et al.* [52]).

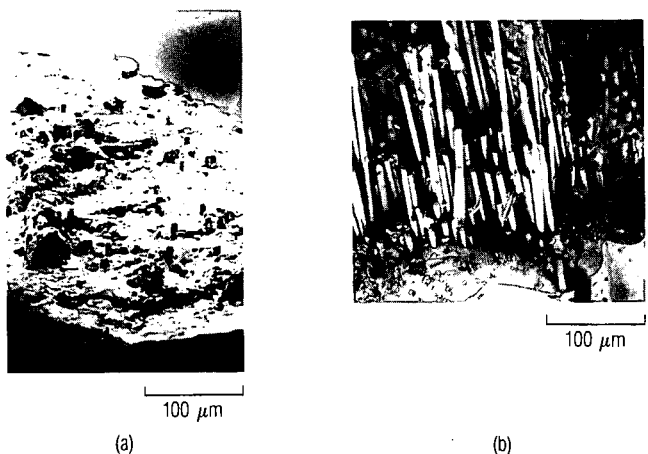


Figure 10. Micrographs of fracture surfaces of (a) undoped and (b) B-doped PAA-derived C/C composites heat-treated to 1100°C [52].

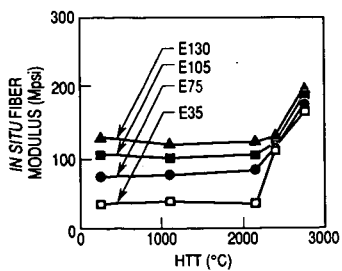


Figure 11. Moduli of composites versus HTT (Zaldivar *et al.* [7]).

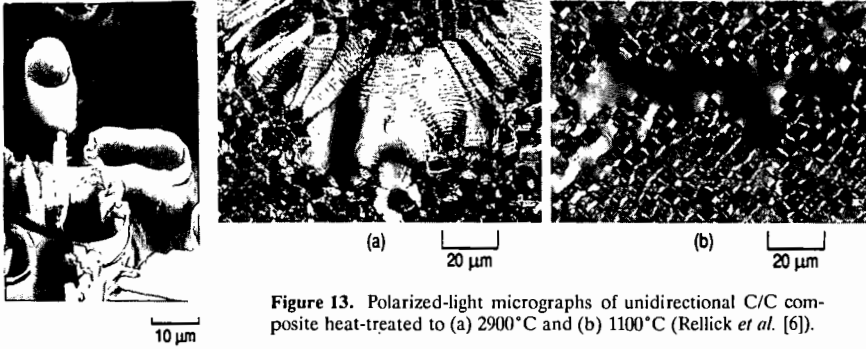


Figure 12. Fracture surface of E105 composite to 2750°C HTT, showing matrix sheath tube (Zaldivar *et al.* [7]).

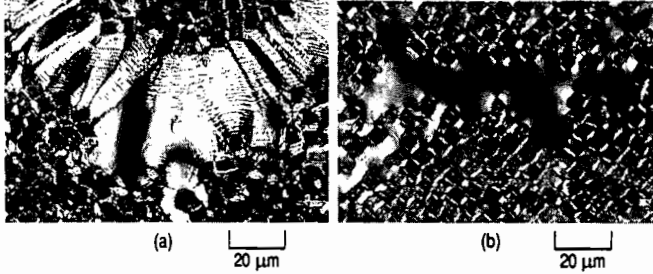


Figure 13. Polarized-light micrographs of unidirectional C/C composite heat-treated to (a) 2900°C and (b) 1100°C (Rellick *et al.* [6]).

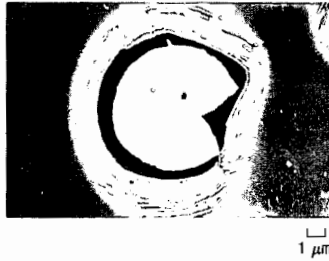


Figure 14. SEM micrograph of PX-7 filament embedded in PAA-derived carbon matrix heat-treated to 2750°C.

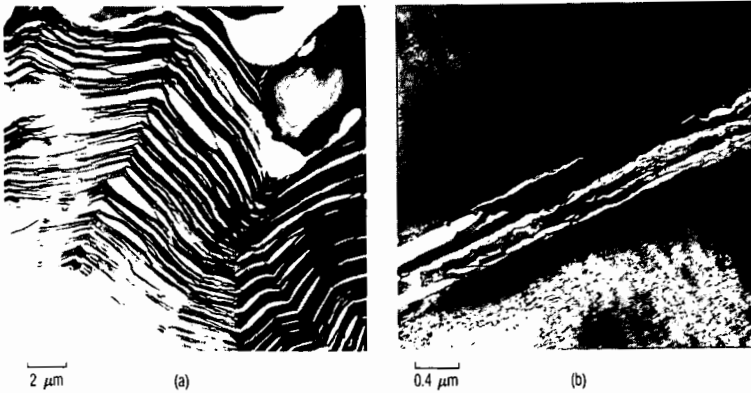


Figure 15. TEM bright-field images of C/C resin-matrix-derived unidirectional composite: (a) transverse and (b) longitudinal sections (Rellick and Adams [56]).

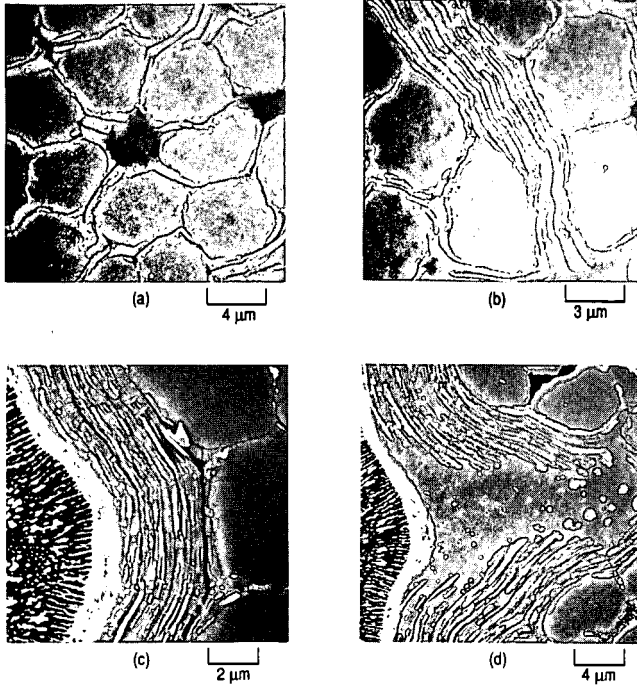


Figure 16. SEMs of ion-etched unidirectional C/Cs heat-treated to 2900°C (Rellick *et al.* [6]).



Figure 17. SEM fracture surface of T50/SC1008 heat-treated to 2900°C [6].

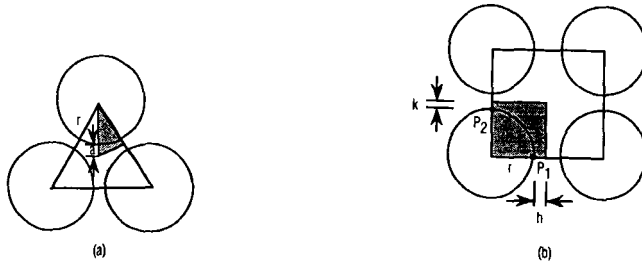


Figure 18. Schematic of the local packing arrangement of (a) three and (b) four fibers. Shaded area denotes region for which stresses are calculated [6].

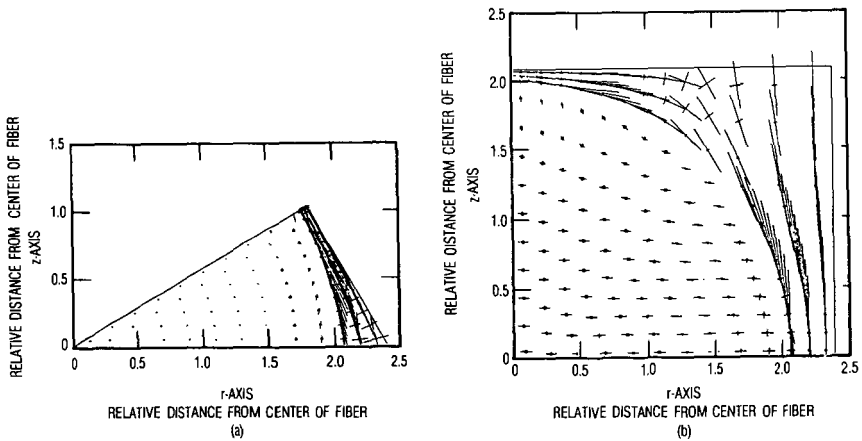


Figure 19. Computer plot of the directions and relative magnitudes of the matrix stresses in the plane of the fiber of various points, relative to Figs. 18a and b [6].